Journal of Alloys and Compounds 509 (2011) 5356–5363

Contents lists available at ScienceDirect

Journal of Alloys and Compounds

journal homepage: www.elsevier.com/locate/jallcom

Dielectric and ferroelectric properties and electric conductivity of sol–gel derived PBZT ceramics

D. Bochenek, R. Skulski*, P. Wawrzała, D. Brzezińska

University of Silesia, Department of Materials Science, 2, Śnieżna St., 41-200 Sosnowiec, Poland

ARTICLE INFO

Article history:
Received 4 June 2010
Received in revised form 4 February 2011
Accepted 7 February 2011
Available online 16 February 2011

Keywords:
Ferroelectric
Relaxor
Ceramics
Phase transition
Hysteresis loop

ABSTRACT

$(Pb_{1-x}Ba_x)(Zr_{1-y}Ti_y)O_3$ (PBZT) is a solid solution in which ferroelectric, relaxor or antiferroelectric properties are observed depending on composition. The substitution of Ba^{2+} into A position of the perovskite structure leads to the decrease in phase transition temperature and it gradually leads to relaxor properties. The majority of papers describe PBZT obtained from oxides. We report the results of the investigation of the properties and phase transitions of $(Pb_{1-x}Ba_x)(Zr_{0.65}Ti_{0.35})O_3$ ceramics with $x = 0.09$, 0.25 and 0.35 obtained by the sol–gel method with final free sintering (FS) at 1573 K/4 h and by the hot pressing (HP) method at 1473 K/2 h/20 MPa. Unlike pure PZT, the properties of HP-PBZT samples obtained at lower (1473 K) temperature are a little inferior than FS samples. It is probably related to the fact that barium requires higher final sintering temperatures.

We present the results of XRD and dielectric measurements vs. temperature for PBZT ceramics. On the basis of dielectric measurements a.c. conductivity and activation energies have been calculated. In agreement with earlier literature data, we note that with the increasing Ba content T_m decreases and the maximum of $\varepsilon(T)$ is wider. However, we do not observe a shift of T_m with increasing frequency. The room $P(E)$ hysteresis loops become more narrow and the polarization is smaller. The increase in dielectric losses with increasing temperature makes the measurement of hysteresis loops at low frequencies and high temperatures difficult.

1. Introduction

Though PZT-type ferroelectrics are known and applicated from many years numerous relevant papers have been published in last years (for example [1–3]). $(Pb_{1-x}Ba_x)(Zr_{1-y}Ti_y)O_3$ (PBZT) solid solutions are discussed at length in the literature with many practical purposes [4,5]. The phase diagram of a solid PBZT solution was described in [6]. The substitution of Pb^{2+} ions by Ba^{2+} ions in PBZT leads to important changes in dielectric properties investigated in detail in [7–10]. For constant y and increasing x linear decrease in the temperature of maximum dielectric permittivity (T_m) occurs. Moreover, depending on the amount of Ba atoms, a diffuse behaviour and a large frequency dependence of relative dielectric permittivity are observed (i.e. properties typical for relaxor ferroelectrics, RF). For relaxor materials T_m is not the crystal phase transition temperature. At the same time, with increasing Ba content at a constant Zr/Ti proportion, the electric hysteresis becomes more narrow and the value of polarization and coercion field become lower. Usually all these changes are attributed to the fact that the ionic radius of Ba^{2+} ions is about 11% larger than for Pb^{2+}.

In ref. [11], Mir et al. studied the structure of $(Pb_{1-x}Ba_x)(Zr_{0.65}Ti_{0.35})O_3$ ceramics with $0 < x < 0.4$ using synchrotron X-ray powder diffraction data. According to Rietveld refinements, the structure of PBZT ceramics with $x = 0.00$, 0.10 and 0.20 at room temperature was rhombohedral R3c. A phase transition from rhombohedral to cubic was observed at 543 and 463 K for $x = 0.10$ and 0.20, respectively. The refinement for the compositions with $x = 0.30$ and $x = 0.40$ yields a cubic structure within a temperature range of 10–450 K, which is in good agreement with the dielectric properties of these samples. In ref. [12], Mastelaro et al. studied a structural short-range order of $(Pb_{1-x}Ba_x)(Zr_{0.65}Ti_{0.35})O_3$ with $x = 0.3$ and 0.4 using X-ray absorption spectroscopy (XAS) and Raman spectroscopy. XANES results showed that at a very short range order, within the first coordination sphere around the Ti ion, any change can be observed in the spectrum by replacing Pb with Ba ions or changing temperature, contrary to XRD data which indicate rhombohedral to cubic phase transition for $x = 0.0$, 0.10, and 0.20. On the other hand, Raman scattering results showed that even at high Ba concentration ($x = 0.30$ and 0.40) and/or high temperature conditions (cubic phase based on XRD) the Raman spectra show broad bands similar to the tetragonal phase. These

* Corresponding author. Tel.: +48 323689309.
E-mail address: ryszard.skulski@us.edu.pl (R. Skulski).

0925-8388/$ – see front matter © 2011 Elsevier B.V. All rights reserved.
doi:10.1016/j.jallcom.2011.02.046

Table 1
Results of Curie–Weiss fitting for PBZT–FS and PBZT–HP ceramics.

	ρ [g/cm^3]	C_w [K] $T<T_0$	C_w [K] $T>T_0$	T_0 [K]	$\frac{1}{\varepsilon_m}$	T_m [K]	$A\ 10^{-9}$	γ	ΔT
PBZT-FS 9/65/35	7.15	-2.20×10^5	4.09×10^5	548.0	0.00009	582.3	10.10	2.36	530–630
PBZT-FS 25/65/35	6.45	[a]	1.49×10^5	515.0	0.00014	419.1	10.66	2.04	325–600
PBZT-FS 35/65/35	6.59	[a]	1.30×10^5	453.1	0.00028	322.5	3.84	2.18	(70)–570
PBZT-HP 9/65/35	7.72	-1.63×10^5	1.80×10^5	607.6	0.00019	601.5	46.11	1.85	550–650
PBZT-HP 25/65/35	7.18	[a]	2.40×10^5	467.8	0.00023	416.2	8.18	2.02	325–600
PBZT-HP 35/65/35	6.61	[a]	1.66×10^5	426.4	0.00036	351.2	2.01	2.31	(80)–607

[a] Fitting was not possible.

results indicate strongly that at short and medium ranges local symmetry is preserved.

In ref. [13] dielectric and relaxor ferroelectric properties of $Pb_{1-x}Ba_xZr_{0.70}Ti_{0.30}O_3$ with $0.20 < x < 0.30$ were investigated.

All the studies cited above were performed using PBZT ceramics obtained from oxides and carbonides. The main aim of this paper was to obtain $(Pb_{1-x}Ba_x)(Zr_{0.65}Ti_{0.35})O_3$ ceramics with $0.09 \le x \le 0.35$ by the sol–gel method and to investigate the resulting samples. Literature data on sol–gel obtained PBZT concern other compositions (for example [14]) or thin films.

Usually the sol–gel method enables one to obtain reagents with smaller grains to reduce the time and temperature of final sintering. It is very important for lead-containing materials. The main disadvantage is the high cost of organic reagents. In the earlier paper by Bochenek and Wawrzała [15] the details of sol–gel technology and main dielectric parameters of resulting samples were described. In ref. [16] electromechanical properties were investigated. It was stated that for ceramics sintered at higher temperature the grain size, quality of grain shapes and electromechanical properties are improved.

2. Experimental procedures

In this work we obtained samples of $(Pb_{1-x}Ba_x)(Zr_{0.65}Ti_{0.35})O_3$ ceramics with $x = 0.09$, 0.25 and 0.35 denoted as PBZT 9/65/35, PBZT 25/65/35 and PBZT 35/65/35, respectively by the sol–gel method. The powders were obtained using the following reagents: $Pb(CH_3COO)_2$, $Ba(CH_3COO)_2$, $Zr(C_3H_7O)_4$, $Ti(C_3H_7O)_4$. The reagents were weighed in a stoichiometric ratio and heated in a glass vessel. Subsequently, distillation was performed to remove the adventitious reaction product (ester). After cooling down to room temperature hydrolysis and stabilization were performed. As a result gel was obtained which was then powdered. To remove organic residues the powder was dried and calcined. At the next stage the powder was mixed and pressed into pellets at room temperature. Some of the resulting pellets were finally pressureless sintered (free sintered, FS) at 1573 K/4 h while the rest of the pellets were hot pressed (HP) sintered at 1473 K/2 h/20 MPa in air. For electric measurements opposite faces of the samples were coated with silver paste and burnt at 1073 K. The main parameters of the samples obtained using these two methods are shown in Table 1.

X-ray diffraction (XRD) analyses were performed using a Siemens D5000 diffractometer and CuKα filtered radiation with a 0.02° step. The investigation of dielectric permittivity $\varepsilon'(\omega,T)$ and tan $\delta(\omega,T)$ vs. temperature was carried out using a Quadtech 1920 RLC meter. Hysteresis (P–E) loops at various electric field frequencies were investigated with a Sawyer-Tower circuit and a HEOPS-5B6 Matsusada Inc. precision high voltage amplifier. Data were stored on a computer disc using an A/D, D/A transducer card.

3. Results and discussion

The SEM images of the microstructure of PBZT 9/65/35FS and 9/65/35HP are shown in Fig. 1a and b, respectively. For FS ceramics (Fig. 1a) the grain dimensions are smaller in comparison with ref. [17] but comparable with ref. [11]. Grains of HP ceramics (Fig. 1b) are smaller than in refs. [11] and [17] and also smaller in comparison with FS. It is probably a result of exceedingly low temperature in the HP method.

Results of the investigation of XRD patterns are shown in Fig. 2. It is noted that the samples are practically free of the pyrochlore phase; however in the case of 9/65/35 ceramics an additional, unidentified maximum is seen between 60 and 70°. Fig. 3 shows the selected parts of XRD patterns with reflexes 104/110 and 211/21-1. Such reflexes were used for phase identification in ref. [11]. Multipeak decomposition shows that in the case of PBZT 9/65/35 the best results were obtained by the decomposition into two peaks. On the other hand in the case of PBZT 35/65/35 the best results were obtained by fitting to one peak. We can then say that PBZT 9/65/35 is rhombohedral while 35/65/35 is quasicubic. Sample PBZT 25/65/35 shows an intermediate state.

The results of dielectric measurements as a function of temperature for test samples PBZT–FS and PBZT–HP are shown in Fig. 4. It is seen that for PBZT 9/65/35 rather large temperature ranges occur on both sides of T_m with linear dependency $1/\varepsilon'(T)$ (linear Curie–Weiss law) while with increasing Ba content such ranges become smaller. In PBZT 9/65/35 the change of the slope of $1/\varepsilon'(T)$ dependency at about 430 K is also seen. It is probably related to the phase transition between two rhombohedral phases.

Results of $\varepsilon^{-1}(T)$ studies at 10 kHz were fitted to the linear Curie–Weiss law (1) for temperatures far from T_m (i.e. outside the ΔT region in Fig. 4) and to Eq. (2) known as the generalized Curie–Weiss law in the vicinity of T_m (i.e. inside the ΔT region in Fig. 5):

$$\frac{1}{\varepsilon'} = C_W^{-1}(T - T_0) \tag{1}$$

$$\frac{1}{\varepsilon} = \frac{1}{\varepsilon_m} + A\left|T - T_m\right|^{\gamma} \tag{2}$$

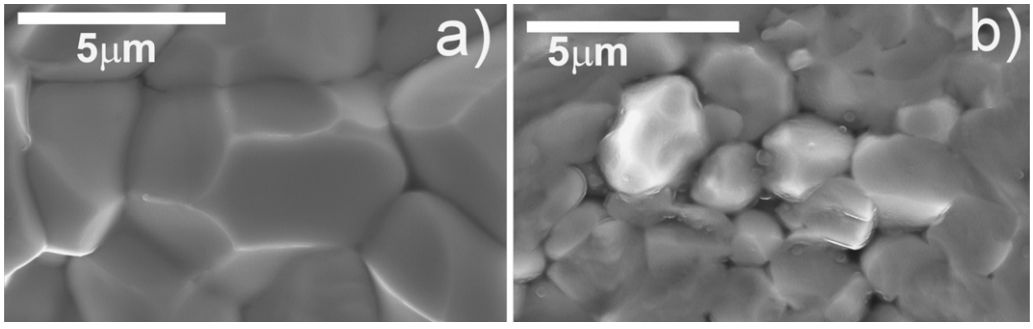

Fig. 1. SEM images of PBZT 9/65/35 microstructure: (a) FS 1573 K/4 h (b) HP 1473 K/2 h/20 MPa.

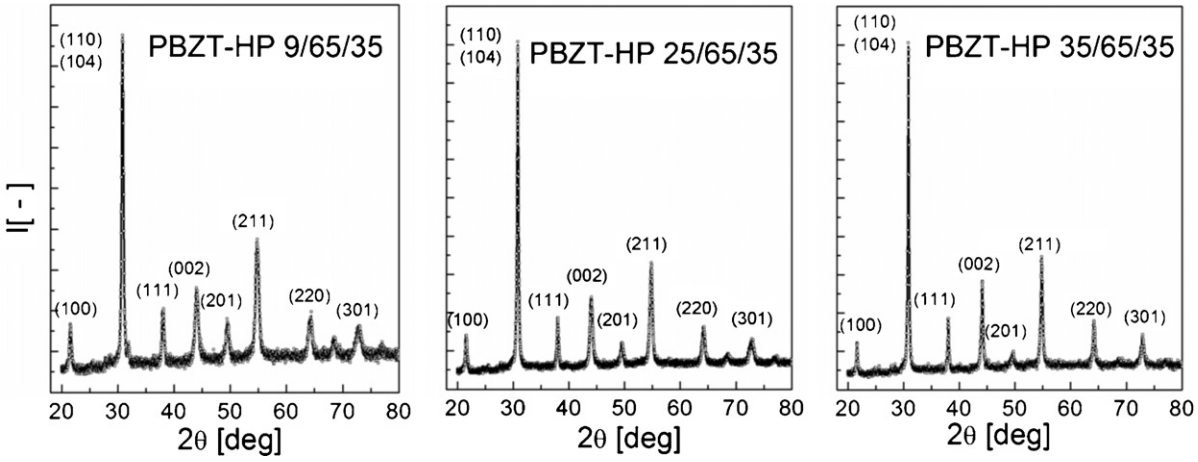

Fig. 2. XRD diffraction patterns for HP sintered samples.

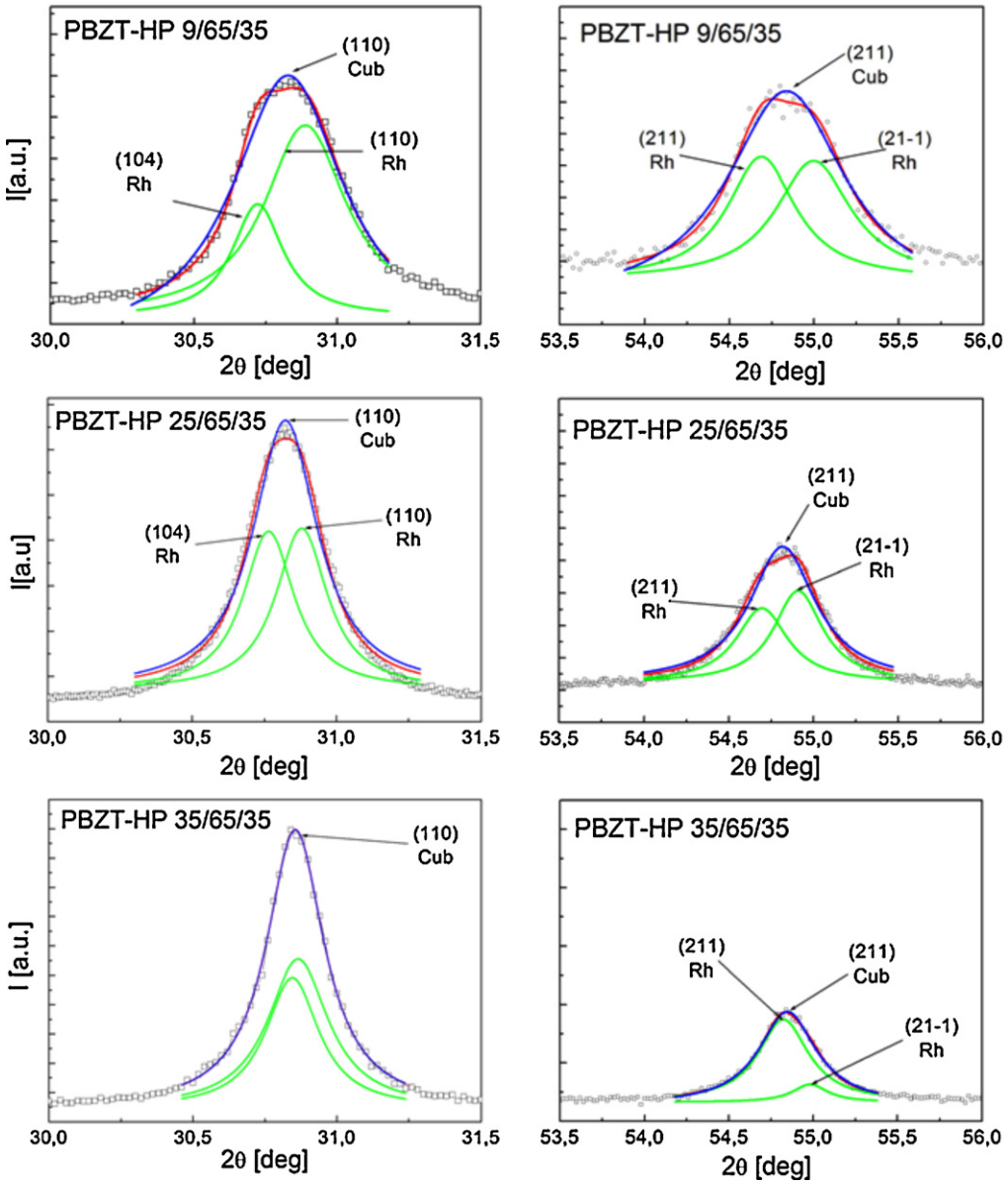

Fig. 3. Selected parts of XRD diffraction patterns obtained at room temperature for HP sintered samples.

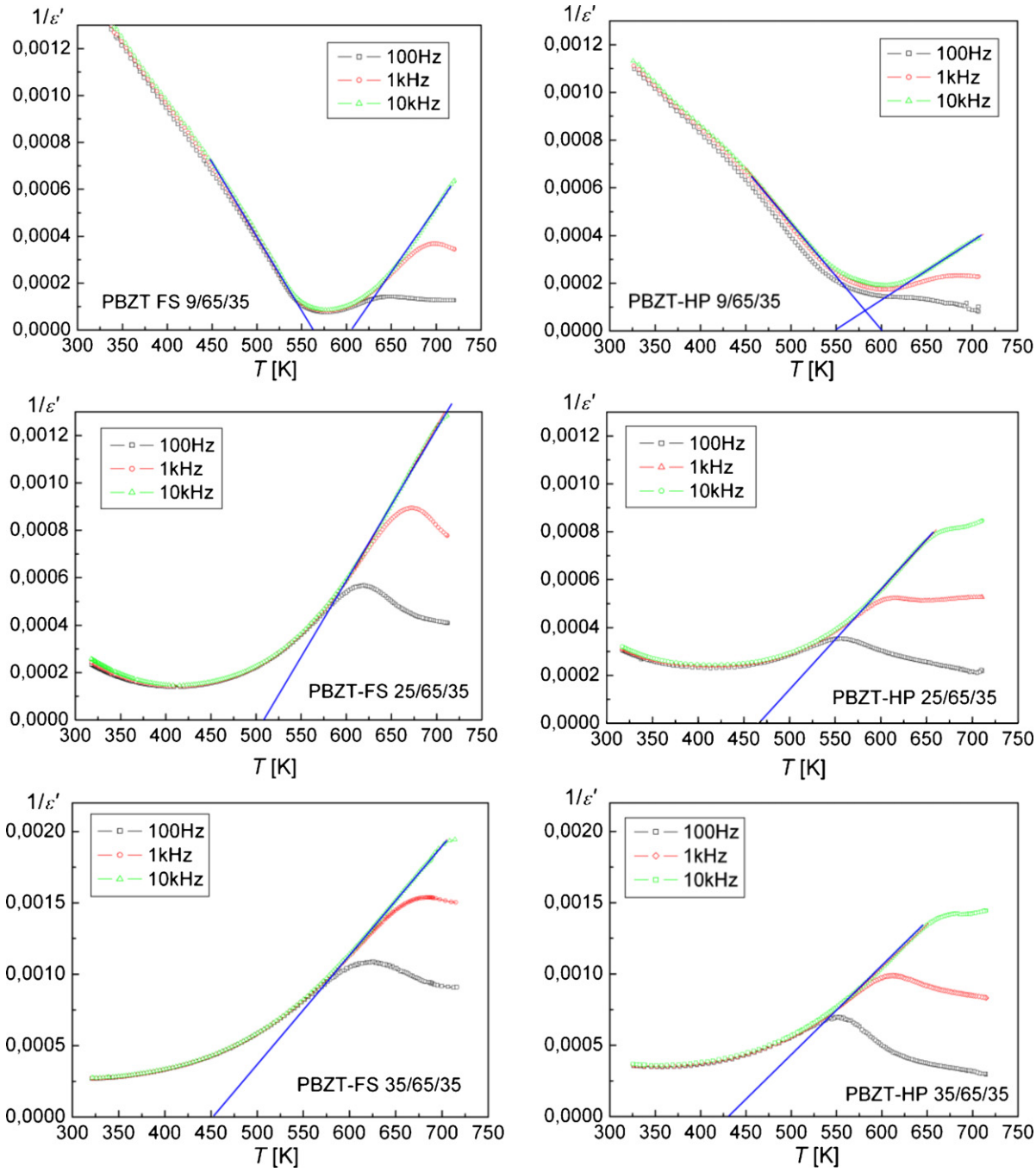

Fig. 4. Curie–Weiss plots for PBZT-FS and PBZT-HP. Blue lines are the results of fitting to the linear Curie–Weiss law (2), see below and Table 1. (For interpretation of the references to color in this figure legend, the reader is referred to the web version of the article.)

where ε' is the real part of dielectric permittivity; C_W is the Curie–Weiss constant; T is the sample temperature; T_0 is the Curie–Weiss temperature; A, γ is the fitting parameters.

The fitting results are shown in Table 1. Comparing the results of dielectric measurements obtained by FS and HP some differences are visible; however, the T_m temperatures are similar. This can be related to differences in electric conductivity between FS and HP samples.

A.c. conductivity σ was calculated using dielectric measurements within a frequency range of 100–20 kHz using the formula:

$$\sigma = \tan\ \delta\omega\varepsilon_0\varepsilon' \tag{3}$$

where $\tan\delta$ is the tangent of dielectric losses angle; $\omega = 2\pi f$ is the frequency.

At very high and very low $\sigma(T)$ temperatures experimental results shown in Fig. 6 can be described by equations:

$$\sigma = \sigma_\infty e^{-(E_a/kT)} \quad \ln\sigma = \ln\sigma_\infty - \frac{E_a}{kT} \tag{4}$$

Using symbols from Fig. 7 we calculated activation energies shown in Table 2. For sample PBZT FS 35/65/35 it was not possible to calculate E_{a2} since our investigations were not performed at temperatures low enough. In Fig. 8 the values of σ vs. frequency for the PBZT ceramics tested are shown. The relationship between a.c.

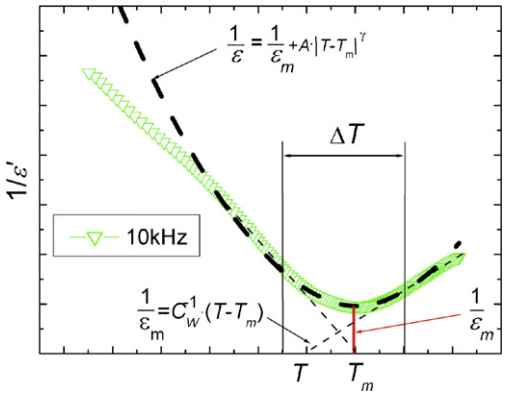

Fig. 5. Schematic presentation of Curie–Weiss fitting and generalized Curie–Weiss fitting.

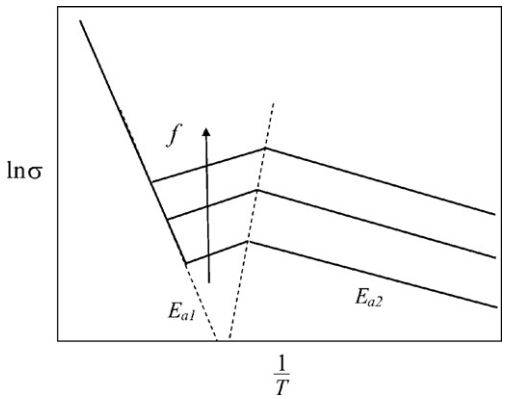

Fig. 7. Schematic diagram showing the symbols used in Table 2.

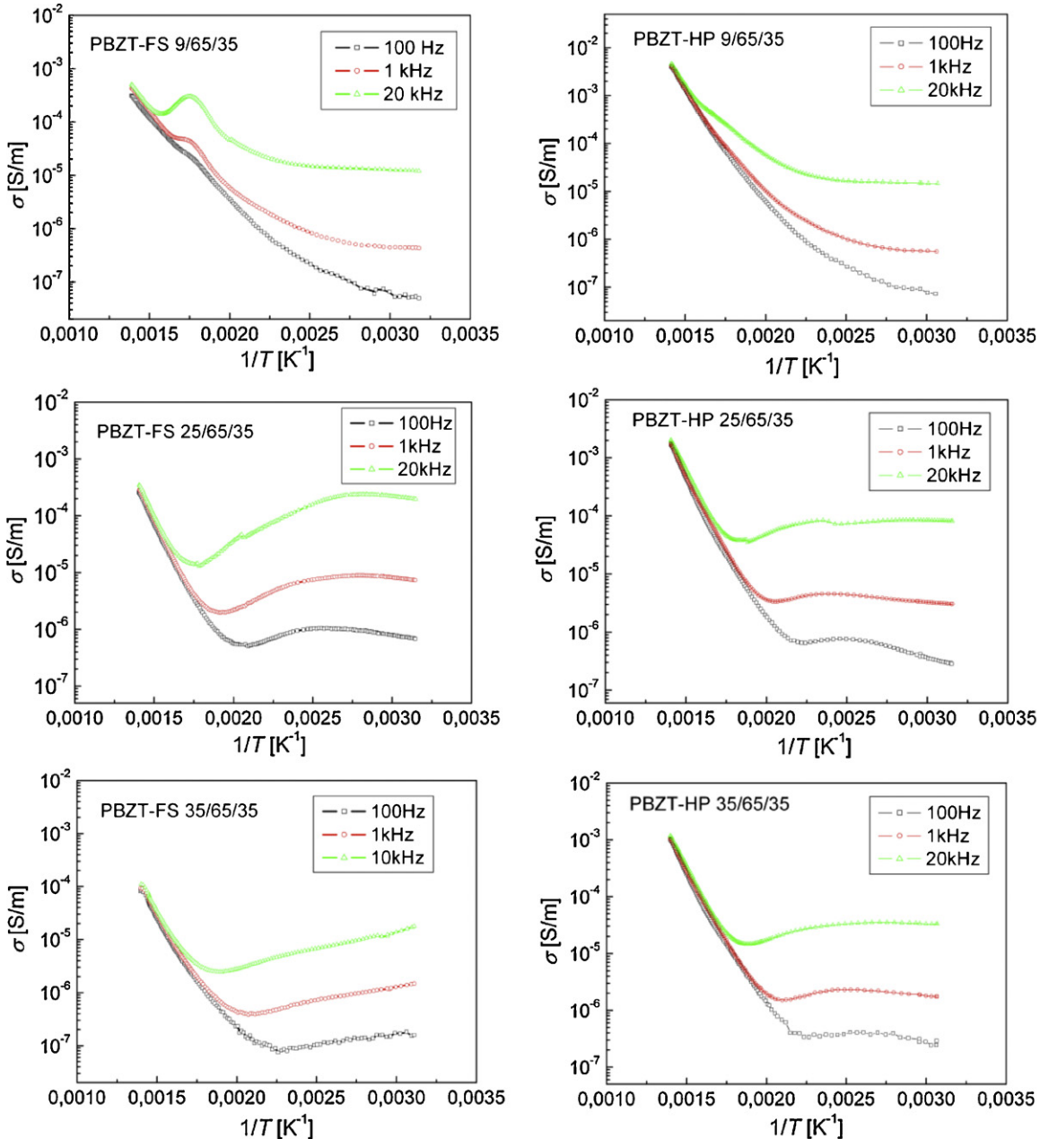

Fig. 6. Results of calculations of a.c. conductivity vs. temperature for PBZT-FS and PBZT-HP.

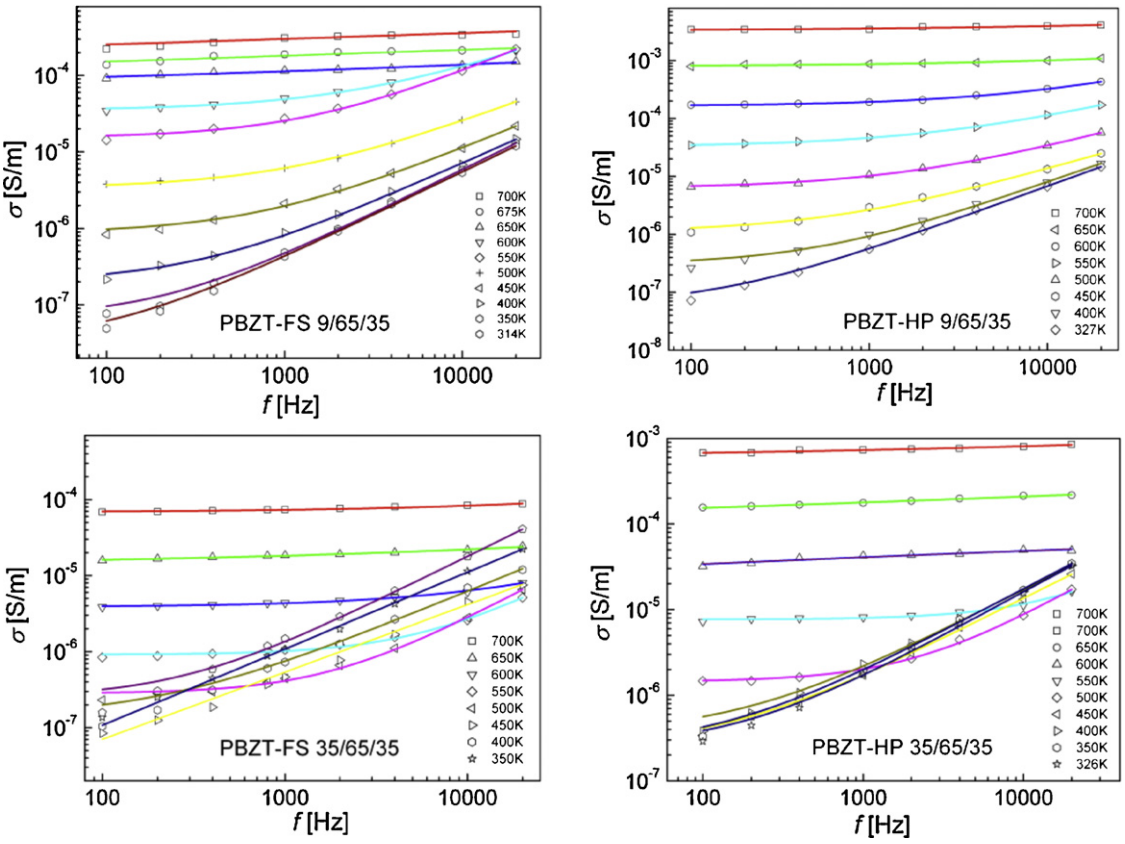

Fig. 8. A.c. conductivity as a function of frequency for PBZT-FS and PBZT-HP ceramics (symbols) and results of fitting to Jonsher's law (lines).

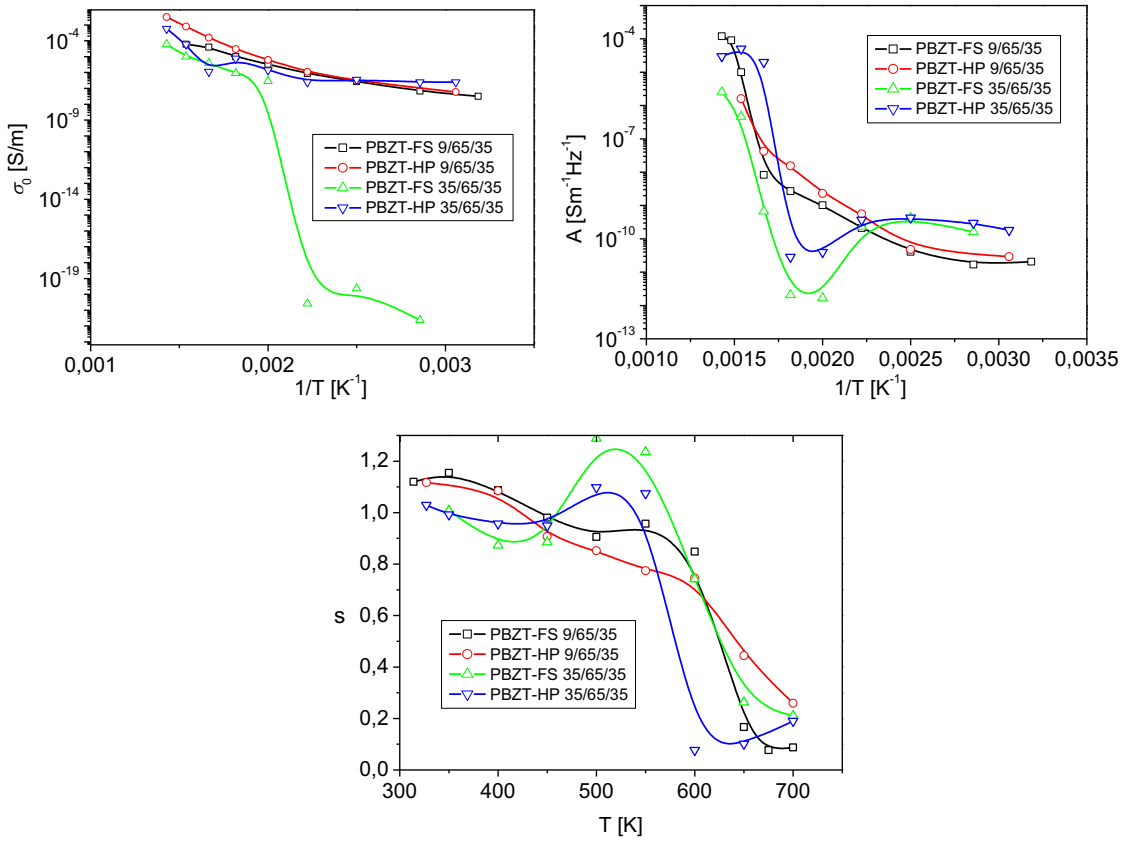

Fig. 9. $\sigma_0(T)$, $A(T)$ and $s(T)$ relationships obtained by fitting experimental results to Jonsher's law (Eq. (5)).

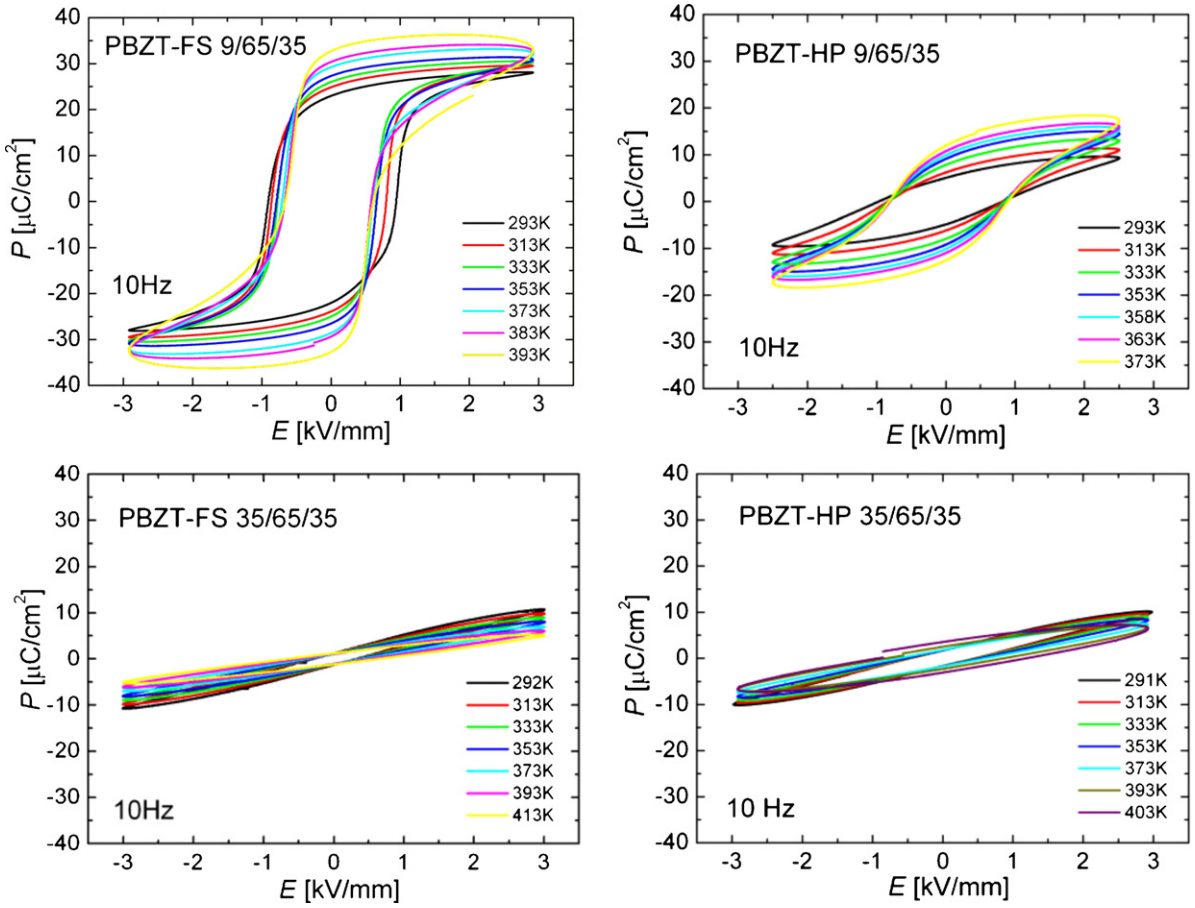

Fig. 10. Changes in hysteresis loops with increasing temperature for PBZT-FS and PBZT-HP ceramics.

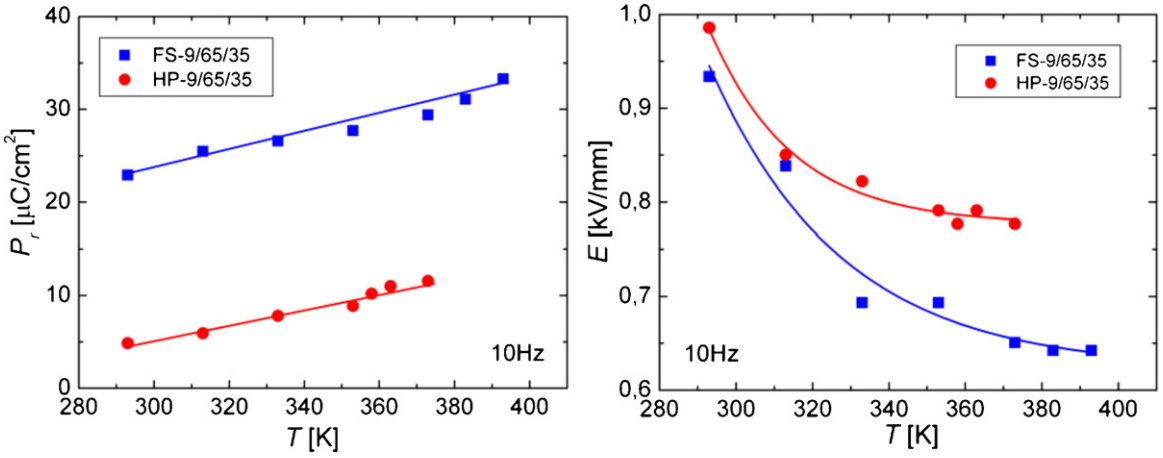

Fig. 11. Dependencies of $P_r(T)$ and $E_C(T)$ for PBZT-FS and PBZT-HP ceramics.

conductivity and frequency are well described by the universal Jonscher's power law [18,19]:

$$\sigma(\omega) = \sigma_0 + A\omega^s \quad (5)$$

where $\sigma(\omega)$ is the a.c. conductivity calculated from Eq. (3), σ_0, A, s is the depending on temperature parameters (i.e. frequency independent). The fitting results are shown in Fig. 9.

At higher temperatures the relationship is close to linear, while at lower temperatures linear parts gradually become narrower. At

Table 2
Activation energies obtained as a result of fitting to Eq. (4).

	E_{a1} [eV]	E_{a2} [eV]		E_{a1} [eV]	E_{a2} [eV]
PBZT-FS 9/65/35	0.671	0.103	PBZT-HP 9/65/35	1.022	0.207
PBZT-FS 25/65/35	1.067	0.088	PBZT-HP 25/65/35	1.027	0.152
PBZT-FS 35/65/35	1.029	–	PBZT-HP 35/65/35	0.933	0.121

low temperatures the differences between FS and HP are rather large in values and in the shape of curves. These differences disappear at high temperatures.

In Fig. 10 $P(E)$ hysteresis loops obtained at 10 Hz and various temperatures are shown. The values of remanent polarization and coercive field at the temperature range from room temperature to about 380 K are shown in Fig. 11. It is noted that for the same x the differences in the shape of hysteresis loops for FS and HP samples are important. For PBZT 9/65/35 the changes in the shape of the hysteresis loop with increasing temperature are typical. For FS samples as well as for HP samples in the range 293–393 K polarization increases with increasing temperature while coercive field decreases. The increase in P_r with increasing temperature is probably not intrinsic, and it may be due to the contribution of leakage current.

4. Conclusions

Our investigation of XRD-diffraction shows that a transition from rhombohedral to cubic (or quasicubic) deformations of elementary cells occur with increasing x, in accordance with earlier literature data in PBZT x/95/65. At the same time the transition to relaxor properties is observed. The relationship between dielectric permittivity and temperature is well described by the so called generalized Curie–Weiss law in the vicinity of T_m and by the normal Curie–Weiss law outside this range.

A.c. conductivity studies show differences between samples with ferroelectric properties and samples with relaxor properties. A.c. conductivity of all samples is described well by the Jonshers universal power law. According to ref. [20] three mechanisms can lead to such electric conductivity behavior:

(I) Excitation of charge carriers into localized states at the edges of valence or conduction band and hopping at energies close to it.
(II) Hopping of carriers in localized states near the Fermi level.
(III) Hopping of carriers among localized sites which could result in Debye-type losses similar to the thermally activated switching of dipoles between two or more directions with different energies.

All mechanisms predict a similar frequency relationship of a.c. conductivity described by the Jonsher equation, but the temperature relationship of a.c. conductivity will be different for the three mechanisms. It is possible to distinguish between them. In our case mechanism (I) probably dominates at high temperatures. At middle temperatures at which conductivity does not change with temperature or decreases with increasing temperature (III) is the possible mechanism, but such probability changes can also be related to the PTC effect described by the Heywang model [21]. At very low temperatures (II) or (III) are the possible mechanisms

The distinct difference between hysteresis loops for PBZT–FS 9/65/35 and PBZT–HP 9/65/35 are probably related to the differences in sample microstructures (see Fig. 1). Almost linear increase in remanent polarization with temperature is probably related to the additional phase transition at about 430 K. This phase transition is also visible at Curie–Weiss plots. In the same temperature range the coercive field decreases exponentially.

It is concluded that the sol–gel method makes it possible to obtain samples with ferroelectric/relaxor properties. Unlike pure PZT, the properties of HP-PBZT samples obtained at lower (1473 K) temperature are a little inferior than FS samples. It is probably related to the fact that barium requires higher final sintering temperatures.

Acknowledgement

Work supported by Polish Grant N N507 480237.

References

[1] X. Chao, D. Ma, R. Gu, Z. Yang, J. Alloys Compd. 491 (2010) 698–702.
[2] B. Tiwari, R.N.P. Choudhary, J. Alloys Compd. 493 (2010) 1–10.
[3] Z. Cao, G. Li, S. Wing Or, J. Zeng, L. Zheng, Q. Yin, J. Alloys Compd. 496 (2010) 13–19.
[4] M.E. Lines, A.M. Glass, Principles and Applications of Ferroelectrics and Related Materials, Clarendon, Oxford, 1977.
[5] B. Jaffe, W.R. Cook, H. Jaffe, Piezoelectric Ceramics, Academic, New York, 1971, p. 239.
[6] T. Ikeda, J. Phys. Soc. Jpn. 14 (1959) 168–174.
[7] G. Li, G.H. Haertling, Ferroelectrics 166 (1995) 31–45.
[8] D.V. Taylor, A.E. Glazounov, et al., Proceedings of Assemblee generale de la SVMT, 1994, pp. 65–68.
[9] Z. Ujma, M. Adamczyk, J. Handerek, J. Eur. Ceram. Soc. 18 (1998) 2007–2201.
[10] M. Adamczyk, Z. Ujma, L. Szymczak, A. Soszyński, J. Koperski, Mater. Sci. Eng., B 136 (2007) 170–176.
[11] M. Mir, V.R. Mastelaro, P.P. Neves, A.C. Doriguetto, D. Garcia, M.H. Lente, J.A. Eirasc, Y.P. Mascarenhasa, Acta Crystallogr., Sect. B: Struct. Sci. 63 (2007) 713–718.
[12] V.R. Mastelaro, A. Mesquita, P.P. Neves, A. Michalowicz, M. Bounif, P.S. Pizani, M.R. Joya, J.A. Eiras, J. Appl. Phys. 105 (2009) 033508.
[13] N. Zhang, Z. Xu, Y. Feng, X. Yao, J. Electroceram. 21 (2008) 609–612.
[14] P. Goel, K.L. Yadav, Indian J. Eng. Mater. Sci. 12 (2005) 552–556.
[15] D. Bochenek, P. Wawrzała, Pol. Ceram. Bull. 91 (2005) 279–286.
[16] D. Bochenek, P. Wawrzała, Pol. Ceram. Bull. 91 (2005) 287–294.
[17] M. Adamczyk, Z. Ujma, L. Szymczak, J. Koperski, Ceram. Int. 31 (2005) 791–794.
[18] A.K. Jonscher, Nature 267 (1977) 673–679.
[19] A.K. Jonscher, J. Mater. Sci. 16 (1981) 2037–2060.
[20] O. Parkash, K.D. Mandal, M.S. Sastry, J. Alloys Compd. 228 (1995) 177–180.
[21] W. Heywang, J. Am. Ceram. Soc. 47 (1964) 484–490.